A&A 492, 769–773 (2008)
DOI: 10.1051/0004-6361:20079203e

Astronomy & Astrophysics

Erratum

Detection of amino acetonitrile in Sgr B2(N)

A. Belloche[1], K. M. Menten[1], C. Comito[1], H. S. P. Müller[1,2], P. Schilke[1], J. Ott[3,4,5], S. Thorwirth[1], and C. Hieret[1]

[1] Max-Planck Institut für Radioastronomie, Auf dem Hügel 69, 53121 Bonn, Germany
e-mail: [belloche;kmenten;ccomito;schilke;sthorwirth;chieret]@mpifr-bonn.mpg.de
[2] I. Physikalisches Institut, Universität zu Köln, Zülpicher Str. 77, 50937 Köln, Germany
e-mail: hspm@ph1.uni-koeln.de
[3] National Radio Astronomy Observatory, 520 Edgemont Road, Charlottesville, VA 22903-2475, USA
e-mail: jott@nrao.edu
[4] California Institute of Technology, 1200 E. California Blvd., Caltech Astronomy, 105-24, Pasadena, CA 91125-2400, USA
[5] CSIRO Australia Telescope National Facility, Cnr Vimiera & Pembroke Roads, Marsfield NSW 2122, Australia

A&A 482, 179–196 (2008), DOI: 10.1051/0004-6361:20079203

ABSTRACT

Aims. A small error was recently found in the program used to compute the integrated intensities in the article Belloche et al. (2008, A&A, 482, 179).
Methods. We provide new versions of Fig. 2 and Tables 3, 5, and 7 with the correct integrated intensities.
Results. The conclusions drawn by Belloche et al. (2008) are not significantly affected by these corrections. Only the mass, density, and central H_2 column density of the compact source emitting the amino acetonitrile lines appear to have been underestimated by 30–40%. This led to an overestimate of the abundance of amino acetonitrile by the same amount. However, the magnitude of this correction is less than the estimated uncertainties on these parameters.

Key words. astrobiology – astrochemistry – line: identification – stars: formation – ISM: individual objects: Sagittarius B2 – errata, addenda

We found recently that some of the integrated intensities published in Belloche et al. (2008) were computed with a program containing a small error in the conversion from the frequency domain to the velocity domain. This error affects only spectra that cover a wide frequency range, i.e. the wideband single-dish 3 mm and 1 mm spectra. As a result, some of the intensities listed in Col. 10 of Table 3, some of the intensities used in Fig. 2, and all single-dish fluxes listed in Col. 13 of Tables 5 and 7 are incorrect (up to 40%). These intensities have to be multiplied by $115.750/\nu$(GHz) for $\nu < 116$ GHz and by $254.176/\nu$(GHz) for $\nu > 200$ GHz, with ν the central frequency of the integration range. The intensities of lines at other frequencies are not affected. We present in this erratum new versions of Fig. 2 and Tables 3, 5, and 7 corrected for this error.

The changes in Fig. 2 are not significant enough to change any of the conclusions we draw from the analysis of the single-dish spectrum because our fitting method was not based on these integrated intensities. Therefore our best fit model is not affected.

The single-dish integrated fluxes of Table 5 are all 40% larger than before. Although this might suggest more extended emission than we initially thought, we actually think this increase does not change our conclusions for the following reason. The transition of cyanoacetylene in the vibrationally excited $v_4 = 1$ state at 81.77 GHz is at such high energy ($E_u/k_B = 1283$ K) that it must come from one or several hot, very compact regions. We can exclude that *several* compact sources contribute to the single-dish flux since only one source is detected in the PdBI map (see Fig. 5j). Since our model does not show any

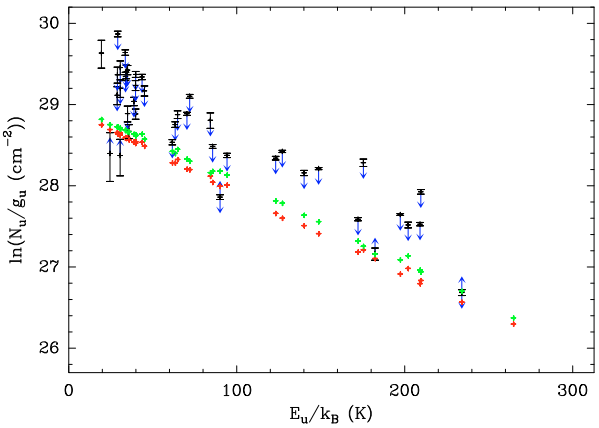

Fig. 2. Population diagram of amino acetonitrile in Sgr B2(N). The red points were computed in the optically thin approximation using the integrated intensities of our best-fit *model* of amino acetonitrile, while the green points were corrected for the opacity. The black points were computed in the optically thin approximation using the integrated intensities of the spectrum *observed* with the IRAM 30 m telescope. The error bars are 1σ uncertainties on N_u/g_u. Blue arrows pointing downwards mark the transitions blended with transitions from other molecules, while blue arrows pointing upwards indicate that the baseline removed in the observed spectrum is uncertain. The arrow length is arbitrary. The measurement corresponding to feature 43 (at $E_u/k_B = 265$ K) is not shown since the integrated intensity measured toward Sgr B2(N) is negative, due to the blend with CN absorption lines.

Table 3. Transitions of amino acetonitrile detected toward Sgr B2(N) with the IRAM 30 m telescope.

N^a	Transition	Frequency (MHz)	Unc.^{b} (kHz)	E_l^c (K)	$S\mu^2$ (D^2)	σ^d (mK)	F^e	τ^f	I^g_{obs} (K km s^{-1})	I^g_{AAN} (K km s^{-1})	I^g_{all} (K km s^{-1})	Comments
(1)	(2)	(3)	(4)	(5)	(6)	(7)	(8)	(9)	(10)	(11)	(12)	(13)
1	$9_{0,9}-8_{0,8}$	80 947.479	7	16	60	33	1	0.13	0.93(16)	0.38	0.42	no blend
3	$9_{5,5}-8_{5,4}$	81 700.966	6	47	41	13	2	0.16	1.30(07)	0.67	0.75	partial blend with U-line
4	$9_{5,4}-8_{5,3}$	81 700.967	6	47	41	13	2	–	–	–	–	–
5	$9_{6,3}-8_{6,2}$	81 702.498	5	60	33	13	2	–	–	–	–	–
6	$9_{6,4}-8_{6,3}$	81 702.498	5	60	33	13	2	–	–	–	–	–
7	$9_{4,6}-8_{4,5}$	81 709.838	6	35	48	13	3	0.23	0.55(06)	0.66	0.73	no blend
8	$9_{7,2}-8_{7,1}$	81 709.848	6	76	24	13	3	–	–	–	–	–
9	$9_{7,3}-8_{7,2}$	81 709.848	6	76	24	13	3	–	–	–	–	–
10	$9_{4,5}-8_{4,4}$	81 710.098	6	35	48	13	3	–	–	–	–	–
11	$9_{3,7}-8_{3,6}$	81 733.892	6	27	53	13	4	0.11	0.71(06)	0.32	1.46	blend with CH_3OCH_3 and $HCC^{13}CN$, $v_6 = 1$
12	$9_{3,6}-8_{3,5}$	81 756.174	6	27	53	13	5	0.11	0.55(06)	0.32	0.32	blend with U-line
13	$9_{2,7}-8_{2,6}$	82 224.644	7	21	57	19	6	0.12	0.27(08)	0.36	0.35	uncertain baseline
17	$10_{2,9}-9_{2,8}$	90 561.332	6	25	64	20	7	0.14	0.82(09)	0.52	1.01	blend with weak C_2H_5CN, $v_{13} = 1/v_{21} = 1$
18	$10_{6,4}-9_{6,3}$	90 783.538	6	64	43	14	8	0.28	1.96(06)	1.05	1.40	partial blend with $CH_2(OH)CHO$ and U-line
19	$10_{6,5}-9_{6,4}$	90 783.538	6	64	43	14	8	–	–	–	–	–
20	$10_{5,6}-9_{5,5}$	90 784.281	6	50	50	14	8	–	–	–	–	–
21	$10_{5,5}-9_{5,4}$	90 784.285	6	50	50	14	8	–	–	–	–	–
22	$10_{7,3}-9_{7,2}$	90 790.259	6	80	34	14	9	0.09	0.65(06)	0.32	0.56	blend with U-line
23	$10_{7,4}-9_{7,3}$	90 790.259	6	80	34	14	9	–	–	–	–	–
24	$10_{4,7}-9_{4,6}$	90 798.685	6	39	56	14	10	0.21	1.82(06)	0.81	0.95	blend with U-line
25	$10_{4,6}-9_{4,5}$	90 799.249	6	39	56	14	10	–	–	–	–	–
28	$10_{3,8}-9_{3,7}$	90 829.945	6	31	60	14	11	0.13	1.07(06)	0.47	0.51	blend with U-line also in M?
29	$10_{3,7}-9_{3,6}$	90 868.038	6	31	60	14	12	0.13	0.63(06)	0.47	0.57	partial blend with U-line
30	$10_{2,8}-9_{2,7}$	91 496.108	8	25	64	24	13	0.15	1.09(11)	0.53	0.71	partial blend with CH_3CN, $v_4 = 1$ and U-line
32	$11_{1,11}-10_{1,10}$	97 015.224	8	25	72	21	14	0.18	2.44(09)	0.71	1.78	partial blend with C_2H_5OH and CH_3OCHO
47	$11_{3,9}-10_{3,8}$	99 928.886	6	35	68	14	15	0.15	1.51(06)	0.66	1.24	partial blend with NH_2CN and U-line
48	$11_{3,8}-10_{3,7}$	99 990.567	7	35	68	14	16	0.15	0.93(06)	0.66	0.74	no blend
49	$11_{2,9}-10_{2,8}$	100 800.876	8	29	71	20	17	0.17	1.58(08)	0.75	1.25	partial blend with CH_3CH_3CO, $v = 0$ and U-line
50	$11_{1,10}-10_{1,9}$	101 899.795	8	26	72	34	18	0.18	0.63(14)	0.81	0.88	uncertain baseline
51	$12_{1,12}-11_{1,11}$	105 777.991	8	29	79	43	19	0.20	2.17(18)	0.95	2.88	blend with c-C_2H_4O and C_2H_5CN, $v = 0$
52	$12_{0,12}-11_{0,11}$	107 283.142	8	29	80	24	20	0.21	2.88(10)	1.00	2.01	blend with C_2H_5OH and U-line
53	$12_{2,11}-11_{2,10}$	108 581.408	7	34	77	20	21	0.19	1.59(08)	0.97	1.93	weak blend with C_2H_5OH
58	$12_{5,8}-11_{5,7}$	108 956.206	6	60	66	29	22	0.26	2.33(11)	1.34	3.44	blend with C_2H_5OH
59	$12_{5,7}-11_{5,6}$	108 956.229	6	60	66	29	22	–	–	–	–	–
68	$12_{3,10}-11_{3,9}$	109 030.225	6	40	75	29	23	0.18	1.77(11)	0.89	1.24	partial blend with HC_3N, $v_4 = 1$, C_2H_5OH, and U-line
71	$12_{1,11}-11_{1,10}$	111 076.901	8	31	79	25	24	0.21	1.20(10)	1.08	1.39	slightly shifted?
72	$13_{1,13}-12_{1,12}$	114 528.654	8	34	86	37	25	0.23	2.52(15)	1.23	1.42	partial blend with U-line
84	$15_{10,5}-14_{10,4}$	136 248.969	10	169	55	28	26	0.09	2.10(10)	0.72	1.03	blend with U-line
85	$15_{10,6}-14_{10,5}$	136 248.969	10	169	55	28	26	–	–	–	–	–
89	$15_{4,11}-14_{4,10}$	136 303.599	6	65	93	28	27	0.21	3.99(09)	1.61	4.02	blend with $a(CH_2OH)_2$ and CH_3C_3N
92	$15_{3,13}-14_{3,12}$	136 341.155	6	57	96	28	28	0.24	2.91(10)	1.81	2.22	partial blend with U-line also in M
103	$16_{5,12}-15_{5,11}$	145 325.871	30	83	96	25	29	0.39	2.89(08)	3.30	4.79	uncertain baseline, partial blend with C_2H_5CN, $v_{13} = 1/v_{21} = 1$
104	$16_{5,11}-15_{5,10}$	145 326.209	30	83	96	25	29	–	–	–	–	–
105	$16_{10,6}-15_{10,5}$	145 330.985	40	175	65	25	30	0.11	0.97(07)	0.92	1.02	uncertain baseline
106	$16_{10,7}-15_{10,6}$	145 330.985	40	175	65	25	30	–	–	–	–	–
115	$16_{3,14}-15_{3,13}$	145 443.850	30	63	103	25	31	0.25	4.32(08)	2.18	4.67	blend with C_2H_5CN, $v = 0$ and U-line
118	$16_{1,15}-15_{1,14}$	147 495.789	6	55	106	31	32	0.29	3.27(11)	2.54	11.47	partial blend with $H_3C^{13}CN$, $v_8 = 1$
139	$17_{4,13}-16_{4,12}$	154 542.406	5	79	107	112	33	0.44	13.24(42)	4.63	5.52	blend with U-line
140	$17_{3,15}-16_{3,14}$	154 544.046	5	70	109	112	33	–	–	–	–	–
145	$18_{7,12}-17_{7,11}$	163 454.794	5	127	101	38	34	0.49	10.38(13)	5.32	16.48	partial blend with $HC^{13}CCN$, $v_6 = 1$ and $HCC^{13}CN$, $v_6 = 1$
146	$18_{7,11}-17_{7,10}$	163 454.794	5	127	101	38	34	–	–	–	–	–
147	$18_{8,10}-17_{8,9}$	163 456.136	6	146	96	38	34	–	–	–	–	–
148	$18_{8,11}-17_{8,10}$	163 456.136	6	146	96	38	34	–	–	–	–	–

Table 3. continued.

N^a	Transition	Frequency (MHz)	Unc.^{b} (kHz)	E_l^c (K)	$S\mu^2$ (D^2)	σ^d (mK)	F^e	τ^f	I^g_{obs} (K km s^{-1})	I^g_{AAN} (K km s^{-1})	I^g_{all} (K km s^{-1})	Comments
(1)	(2)	(3)	(4)	(5)	(6)	(7)	(8)	(9)	(10)	(11)	(12)	(13)
149	$18_{9,9}$–$17_{9,8}$	163 470.472	8	166	90	38	35	0.41	15.17(14)	5.57	21.97	partial blend with $HCC^{13}CN$, $v_7 = 1$
150	$18_{9,10}$–$17_{9,9}$	163 470.472	8	166	90	38	35	–	–	–	–	–
151	$18_{6,13}$–$17_{6,12}$	163 473.305	5	111	106	38	35	–	–	–	–	–
152	$18_{6,12}$–$17_{6,11}$	163 473.321	5	111	106	38	35	–	–	–	–	–
155	$18_{11,7}$–$17_{11,6}$	163 525.533	11	216	75	38	36	0.49	10.26(13)	5.27	17.96	blend with HC_3N, $v_4 = 1$
156	$18_{11,8}$–$17_{11,7}$	163 525.533	11	216	75	38	36	–	–	–	–	–
157	$18_{5,14}$–$17_{5,13}$	163 526.183	4	97	110	38	36	–	–	–	–	–
158	$18_{5,13}$–$17_{5,12}$	163 527.171	4	97	110	38	36	–	–	–	–	–
163	$18_{4,15}$–$17_{4,14}$	163 635.326	5	86	114	38	37	0.25	4.07(11)	2.82	5.01	partial blend with C_3H_7CN
164	$18_{3,16}$–$17_{3,15}$	163 640.468	5	78	116	38	38	0.28	4.65(11)	2.98	6.77	partial blend with C_3H_7CN
177	$19_{6,14}$–$18_{6,13}$	172 566.092	50	119	114	44	39	0.38	10.01(14)	4.39	6.43	partial blend with U-line and $HCC^{13}CN$, $v_7 = 1$
178	$19_{6,13}$–$18_{6,12}$	172 566.092	50	119	114	44	39	–	–	–	–	–
227	$23_{4,20}$–$22_{4,19}$	209 272.189	6	130	148	58	40	0.26	8.85(29)	4.62	14.85	blend CH_3CH_3CO, $v = 0$
237	$23_{1,22}$–$22_{1,21}$	209 629.913	9	113	152	45	41	0.32	10.95(24)	5.53	30.87	blend with $HC^{13}CCN$, $v_7 = 2$ and $HCC^{13}CN$, $v_7 = 2$
247	$25_{9,16}$–$24_{9,15}$	227 040.487	50	230	145	96	42	0.29	10.72(55)	9.45	35.32	partial blend with CN absorption and CH_3CH_3CO, $v_t = 1$
248	$25_{9,17}$–$24_{9,16}$	227 040.487	50	230	145	96	42	–	–	–	–	–
249	$25_{8,18}$–$24_{8,17}$	227 045.287	50	210	149	96	42	–	–	–	–	–
250	$25_{8,17}$–$24_{8,16}$	227 045.287	50	210	149	96	42	–	–	–	–	–
251	$25_{10,15}$–$24_{10,14}$	227 055.944	50	254	139	96	43	0.15	-0.72(44)	3.29	3.62	partial blend with CN absorption
252	$25_{10,16}$–$24_{10,15}$	227 055.944	50	254	139	96	43	–	–	–	–	–
253	$25_{7,19}$–$24_{7,18}$	227 079.847	50	191	153	96	44	0.32	12.25(44)	7.16	57.68	blend with $CH_2CH^{13}CN$ and CH_3OH, $v = 0$
254	$25_{7,18}$–$24_{7,17}$	227 079.847	50	191	153	96	44	–	–	–	–	–
273	$25_{2,23}$–$24_{2,22}$	231 485.527	50	138	165	40	45	0.30	13.98(19)	6.27	6.59	blend with U-line?
292	$26_{6,21}$–$25_{6,20}$	236 269.491	60	186	163	37	46	0.36	16.71(18)	8.02	14.17	partial blend with t-C_2H_5OCHO and U-line
293	$26_{6,20}$–$25_{6,19}$	236 270.459	60	186	163	37	46	–	–	–	–	–
306	$28_{0,28}$–$27_{0,27}$	244 765.968	21	160	186	39	47	0.28	9.93(19)	6.62	10.35	blend with $CH_3{}^{13}CH_2CN$, $v = 0$ and U-line
322	$27_{6,22}$–$26_{6,21}$	245 378.722	10	197	170	72	48	0.35	17.29(36)	8.29	22.20	blend with $^{13}CH_3CH_2CN$, $v = 0$?
323	$27_{6,21}$–$26_{6,20}$	245 380.146	10	197	170	72	48	–	–	–	–	–
368	$29_{9,20}$–$28_{9,19}$	263 364.923	22	277	174	74	49	0.26	6.49(37)	8.51	9.17	baseline problem?, blend with U-line
369	$29_{9,21}$–$28_{9,20}$	263 364.923	22	277	174	74	49	–	–	–	–	–
370	$29_{10,19}$–$28_{10,18}$	263 368.355	26	300	170	74	49	–	–	–	–	–
371	$29_{10,20}$–$28_{10,19}$	263 368.355	26	300	170	74	49	–	–	–	–	–
384	$29_{6,24}$–$28_{6,23}$	263 604.573	12	221	184	74	50	0.28	9.92(36)	8.81	14.21	baseline problem?, partial blend with CH_3CH_3CO, $v_t = 1$ and CH_3OCH_3
385	$29_{6,23}$–$28_{6,22}$	263 607.689	12	221	184	74	50	–	–	–	–	–
398	$29_{4,26}$–$28_{4,25}$	264 055.836	13	197	189	108	51	0.22	17.67(49)	5.92	14.22	partial blend with C_2H_5CN, $v = 0$ and CH_3CH_3CO, $v = 0$

Notes: [a] Numbering of the observed transitions with $S\mu^2 > 20$ D^2 (see Table 2). [b] Frequency uncertainty. [c] Lower energy level in temperature units (E_l/k_B). [d] Calculated rms noise level in T_{mb} scale. [e] Numbering of the observed features. [f] Peak opacity of the amino acetonitrile modeled feature. [g] Integrated intensity in T_{mb} scale for the observed spectrum (Col. 10), the amino acetonitrile model (Col. 11), and the model including all molecules (Col. 12). The uncertainty in Col. 10 is given in parentheses in units of the last digit.

contamination by other molecules in the single-dish spectrum of this transition (see Fig. 4a), we expect the Plateau de Bure (PdBI) interferometric flux to be equal to the single-dish flux. Therefore the flux loss of 45% appearing in the new table for this transition points to an inaccurate intercalibration of the single-dish and PdBI data on the order of 45% instead.

To solve this intercalibration problem, we compared our PdBI continuum measurements to the continuum measurements done by Liu & Snyder (1999) at 85 GHz with the Berkeley-Illinois-Maryland Array (BIMA) with a beam of 1.2″× 0.5″ (*HPBW*) at a position angle of 15° [1]. These authors measured a flux of 4.38 Jy over a vertical box of size 3.2″×4.8″ containing the 4 sources F1 to F4 in the Sgr B2(M) region. To account for the larger PdBI beam ($HPBW = 3.4'' \times 0.8''$ with a position angle at 10°), we integrated the PdBI emission over a slightly larger box of size 3.2″ × 5.8″. After correction for primary beam attenuation, we find an integrated flux of 2.7 Jy when the box is centered on F3, and 3.1 Jy when it is centered 0.7″ to the south of F3. Therefore, the PdBI flux is ∼30 to 40% smaller than the BIMA flux. The comparison for the SgrB2(N) region is more difficult to perform because Liu & Snyder (1999) list

[1] To compute the continuum fluxes in Belloche et al. (2008), we avoided the spectral ranges with detected line emission that otherwise would contaminate the continuum fluxes (by up to 10% toward Sgr B2(N)). Liu & Snyder (1999) did the same (S.-Y. Liu, private communication).

Table 5. Measurements obtained toward Sgr B2(N) with the IRAM Plateau de Bure interferometer at 82 GHz.

Molecule	F^a	$f_{\rm min}{}^b$ (MHz)	$f_{\rm max}{}^b$ (MHz)	σ^c (Jy/beam km s^{-1})	$F_{\rm peak}{}^d$	$\Delta\alpha^d$ ($''$)	$\Delta\delta^d$ ($''$)	$\theta_{\rm maj}^{fwhm\ d}$ ($''$)	$\theta_{\rm min}^{fwhm\ d}$ ($''$)	PA^d (°)	$\Phi^e_{\rm PdBI}$ (Jy km s^{-1})	$\Phi^f_{\rm 30\,m}$ (Jy km s^{-1})
(1)	(2)	(3)	(4)	(5)	(6)	(7)	(8)	(9)	(10)	(11)	(12)	(13)
AAN	F2	81 700.21	81 703.33	0.09	0.68	−1.60 ± 0.05	0.30 ± 0.22	3.9 ± 0.4	2.00 ± 0.10	20.5 ± 0.1	1.76	4.10
AAN	F3	81 708.02	81 712.08	0.10	0.68	−1.25 ± 0.06	0.02 ± 0.24	3.8 ± 0.5	1.39 ± 0.12	10.1 ± 0.0	1.24	2.49
AAN	F4	81 732.71	81 734.90	0.06	0.44	−1.70 ± 0.06	0.35 ± 0.24	3.6 ± 0.5	1.54 ± 0.12	14.0 ± 0.0	0.86	1.38
AAN	F5	81 754.90	81 757.40	0.06	0.24	−1.52 ± 0.10	0.03 ± 0.44	3.2 ± 0.9	1.20 ± 0.21	12.5 ± 1.1	0.30	1.63
AAN	F6	82 223.46	82 226.27	0.06	0.43	−1.43 ± 0.06	0.28 ± 0.24	3.5 ± 0.5	1.54 ± 0.11	6.0 ± 0.4	0.79	1.37
Reference		81 704.27	81 707.08	0.07	...	...	...	...	...	...	...	...
C_2H_5CN	HV	81 741.77	81 744.90	0.11	2.05	−1.64 ± 0.02	5.58 ± 0.09	3.8 ± 0.2	1.50 ± 0.04	5.7 ± 0.0	4.07	9.03
C_2H_5CN	LV	81 745.21	81 749.27	0.15	2.82	−1.74 ± 0.02	0.46 ± 0.09	3.8 ± 0.2	2.87 ± 0.04	13.7 ± 0.0	10.43	18.32
$HC^{13}CCN$ $v_7 = 1$		81 726.15	81 728.96	0.09	2.20	−1.35 ± 0.02	0.60 ± 0.07	3.7 ± 0.1	1.68 ± 0.03	12.6 ± 0.0	4.98	6.81
HC_3N $v_4 = 1$		81767.71	81 771.15	0.10	2.14	−1.43 ± 0.02	0.28 ± 0.08	3.6 ± 0.2	1.35 ± 0.04	9.9 ± 0.0	3.78	5.45
HC_3N $v_7 = 1^g$	HV	82 196.27	82 198.77	0.25	6.17	−2.16 ± 0.02	0.69 ± 0.07	4.0 ± 0.1	1.84 ± 0.03	16.2 ± 22.5	16.05	33.63
					3.36	−1.50 ± 0.03	5.25 ± 0.12	4.0 ± 0.2	1.36 ± 0.06	5.5 ± 22.5	5.35	...
HC_3N $v_7 = 1$	LV	82 199.40	82 201.58	0.36	9.06	−1.67 ± 0.02	0.42 ± 0.07	3.7 ± 0.1	2.50 ± 0.03	10.2 ± 22.5	31.04	47.15
HC_3N $v_7 = 1$	BW	82 202.52	82 203.77	0.12	3.37	−0.71 ± 0.01	0.24 ± 0.06	3.1 ± 0.1	2.77 ± 0.03	45.0 ± 0.0	11.75	17.44
CH_3OCHO		82 242.21	82 245.33	0.10	0.67	−2.83 ± 0.06	1.23 ± 0.26	4.8 ± 0.5	2.58 ± 0.12	9.5 ± 22.5	2.83	9.32

[a] Feature numbered like in Col. 8 of Table 3 for amino acetonitrile (AAN). HV and LV mean "high" and "low" velocity components, respectively, and BW means blueshifted linewing. [b] Frequency range over which the intensity was integrated. [c] Noise level in the integrated intensity map shown in Fig. 5. [d] Peak flux, offsets in right ascension and declination with respect to the reference position of Fig. 5, major and minor diameters (*FWHM*), and position angle (East from North) derived by fitting an elliptical 2D Gaussian to the integrated intensity map shown in Fig. 5. The uncertainty in Col. 11 is the formal uncertainty given by the fitting routine GAUSS_2D, while the uncertainties correspond to the beam size divided by two times the signal-to-noise ratio in Cols. 7 and 8 and by the signal-to-noise ratio in Cols. 9 and 10. [e] Flux spatially integrated over the region showing emission in the integrated intensity map of Fig. 5. [f] Integrated flux of the 30 m spectrum computed over the frequency range given in Cols. 3 and 4. [g] The two emission peaks of Fig. 5k were fitted separately.

Table 7. Measurements obtained toward Sgr B2(N) with the Australia Telescope Compact Array at 91 GHz.

Molecule[a]	Conf.[b]	$f_{\rm min}{}^c$ (MHz)	$f_{\rm max}{}^c$ (MHz)	σ^d (Jy/beam km s^{-1})	$F_{\rm peak}{}^e$	$\Delta\alpha^e$ ($''$)	$\Delta\delta^e$ ($''$)	$\theta_{\rm maj}^{fwhm\ e}$ ($''$)	$\theta_{\rm min}^{fwhm\ e}$ ($''$)	PA^e (°)	$\Phi^f_{\rm ATCA}$ (Jy km s^{-1})	$\Phi^g_{\rm 30\,m}$ (Jy km s^{-1})
(1)	(2)	(3)	(4)	(5)	(6)	(7)	(8)	(9)	(10)	(11)	(12)	(13)
AAN F7	E	90 558.99	90 563.99	0.12	0.87	−2.32 ± 0.20	−0.22 ± 0.13	2.9 ± 0.4	2.2 ± 0.3	29.2 ± 0.1	1.12	3.91
AAN F7	I	90 559.05	90 564.05	0.15	1.47	−1.94 ± 0.20	0.58 ± 0.10	3.6 ± 0.4	2.7 ± 0.2	−79.8 ± 1.5	1.73	3.91
AAN F7	C	90 561.48	90 564.23	0.10	1.53	−0.96 ± 0.21	0.71 ± 0.17	7.0 ± 0.4	4.8 ± 0.3	−80.3 ± 0.0	1.37	2.29
AAN F7	M	90 559.13	90 563.96	0.12	1.19	−2.10 ± 0.16	0.25 ± 0.10	3.1 ± 0.3	2.7 ± 0.2	83.5 ± 0.0	1.71	3.78
AAN F7	A	90 562.03	90 563.96	0.06	0.61	−1.23 ± 0.15	0.26 ± 0.10	5.3 ± 0.3	3.3 ± 0.2	87.1 ± 22.5	1.37	1.28
AAN F8	E	90 781.27	90 786.77	0.21	1.22	−1.94 ± 0.24	−0.18 ± 0.16	3.8 ± 0.5	2.1 ± 0.3	45.0 ± 0.0	1.70	9.22
AAN F9	E	90 788.02	90 792.02	0.09	0.45	−1.70 ± 0.29	−0.06 ± 0.19	3.4 ± 0.6	1.9 ± 0.4	45.0 ± 0.1	0.49	2.72
AAN F9	I	90 788.11	90 792.11	0.13	0.97	−1.77 ± 0.26	0.23 ± 0.13	3.6 ± 0.5	2.2 ± 0.3	−84.0 ± 0.0	1.01	2.72
AAN F9	C	90 790.54	90 792.04	0.10	2.00	−1.25 ± 0.16	0.49 ± 0.13	6.1 ± 0.3	5.8 ± 0.3	−45.0 ± 0.0	1.86	2.02
AAN F9	M	90 788.04	90 792.16	0.10	0.85	−1.67 ± 0.17	0.02 ± 0.11	3.1 ± 0.3	2.4 ± 0.2	75.9 ± 0.1	1.07	2.72
AAN F9	A	90 790.95	90 792.16	0.05	0.63	−1.26 ± 0.14	0.23 ± 0.09	4.8 ± 0.3	3.9 ± 0.2	84.5 ± 0.0	1.51	1.67
AAN F10	E	90 796.52	90 800.77	0.16	1.17	−2.51 ± 0.20	0.02 ± 0.13	2.7 ± 0.4	2.2 ± 0.3	−81.2 ± 0.2	1.38	8.27
AAN F10	I	90 796.61	90 800.86	0.10	0.93	−1.81 ± 0.21	0.20 ± 0.11	3.3 ± 0.4	2.0 ± 0.2	82.3 ± 0.0	0.79	7.89
AAN F10	C	90 796.54	90 800.79	0.15	3.36	−1.08 ± 0.15	0.28 ± 0.12	6.6 ± 0.3	4.9 ± 0.2	−77.7 ± 0.0	2.78	8.27
AAN F10	M	90 796.52	90 800.88	0.13	1.32	−2.28 ± 0.15	0.03 ± 0.09	2.9 ± 0.3	2.2 ± 0.2	83.7 ± 22.5	1.42	8.27
AAN F10	A	90 796.52	90 800.88	0.13	1.82	−1.66 ± 0.12	0.12 ± 0.08	4.5 ± 0.2	3.1 ± 0.2	−89.3 ± 22.5	3.24	8.27
$HC^{13}CCN$ $v_7 = 1$ HV	I	90 804.36	90 805.36	0.05	0.49	−1.94 ± 0.20	5.16 ± 0.10	3.0 ± 0.4	2.0 ± 0.2	84.4 ± 0.0	0.41	3.05
$HC^{13}CCN$ $v_7 = 1$ LV	I	90 806.11	90 809.36	0.14	2.74	−1.56 ± 0.10	0.55 ± 0.05	3.7 ± 0.2	2.1 ± 0.1	83.6 ± 0.0	2.69	13.13
$HC^{13}CCN$ $v_7 = 1$ LV	C	90 806.04	90 809.29	0.15	4.98	−1.71 ± 0.10	0.25 ± 0.08	7.1 ± 0.2	4.4 ± 0.2	−83.8 ± 0.0	4.12	13.13
CH_3OH $v_t = 1$ HV	I	90 809.61	90 811.11	0.09	1.52	−1.85 ± 0.12	5.23 ± 0.06	3.7 ± 0.2	2.1 ± 0.1	−85.7 ± 0.1	1.54	8.35
CH_3OH $v_t = 1$ LV	I	90 812.36	90 814.11	0.11	1.60	−1.84 ± 0.13	0.44 ± 0.06	3.8 ± 0.3	3.6 ± 0.1	23.7 ± 22.5	2.72	13.26
CH_3OH $v_t = 1$ LV	C	90 812.29	90 814.29	0.12	5.22	−1.86 ± 0.08	−0.03 ± 0.06	7.1 ± 0.2	4.5 ± 0.1	−77.9 ± 0.0	4.29	13.26

[a] For amino acetonitrile (AAN), we give the feature number like in Col. 8 of Table 3. For the other molecules, HV and LV mean high and low velocity component, respectively. [b] Interferometer configuration: E: extended (H 214), I: intermediate (H 168), C: compact (H 75), M: mixed (H 214 + H 168), A: all (H 214 + H 168 + H 75). [c] Frequency range over which the intensity was integrated. [d] Noise level in the integrated intensity map shown in Fig. 7. [e] Peak flux, offsets in right ascension and declination with respect to the reference position of Fig. 7, major and minor diameters (*FWHM*), and position angle (East from North) derived by fitting an elliptical 2D Gaussian to the integrated intensity map shown in Fig. 7. The uncertainty in Col. 11 is the formal uncertainty given by the fitting routine GAUSS_2D, while the uncertainties correspond to the beam size divided by two times the signal-to-noise ratio in Cols. 7 and 8 and by the signal-to-noise ratio in Cols. 9 and 10. [f] Flux spatially integrated over the region showing emission in the integrated intensity map of Fig. 7. [g] Integrated flux of the 30 m spectrum computed over the frequency range given in Cols. 3 and 4.

fluxes integrated over boxes smaller than the PdBI beam. They found a flux of 0.90 Jy over a box of size $2.8'' \times 3.2''$ centered on K2. An integration over a larger box of size $2.8'' \times 4.5''$ to account for the larger PdBI beam yields a PdBI flux of 0.72 Jy, i.e. ∼20% smaller than the BIMA flux. However, the PdBI flux is contaminated by emission from K3 and the actual PdBI flux for K2 is most likely even smaller.

As a result, we think that all PdBI fluxes listed in Table 5 are underestimated by ∼30−40%. Since the integration error underestimated the single-dish fluxes by about the same amount, our conclusions about the compact size of the amino acetonitrile emission remain unchanged. On the other hand, the underestimate of the continuum flux led to an underestimate by ∼30−40% of the H_2 column density, mass, and density in Sect. 3.6, which implies an overestimate of the amino acetonitrile abundance by the same amount. We note, however, that the uncertainty on the quantities derived from the continuum emission is close to a factor of 2, dominated by the uncertainties on the dust properties as we mentioned in Sect. 3.6.

Finally, the single-dish integrated fluxes of Table 7 are all ∼30% larger than before. The ATCA interferometric flux of feature F7 in the full set of configurations (labeled A in Col. 2) now agrees within 10% with the single-dish flux. This indicates that no emission was filtered out by the interferometer, i.e. that all the emission of amino acetonitrile is from a compact source. This agreement also supports our finding that the fluxes measured with the PdBI were too low, while the calibration of the single-dish spectra should be correct.

As a conclusion, the errors reported here do not change the conclusions we draw about the emission of amino acetonitrile in Sgr B2(N). Only the abundance may have been overestimated by ∼30−40%, which is still within its uncertainty.

Acknowledgements. We thank Sheng-Yuan Liu for providing very useful information about the way the flux integration was performed on the BIMA data, and Roberto Neri for helpful discussion about the calibration of the PdBI data.

References

Belloche, A., Menten, K. M., Comito, C., et al. 2008, A&A, 482, 179
Liu, S.-Y., & Snyder, L. E. 1999, ApJ, 523, 683